Effect of solvent motions on the dynamics of the Diels-Alder reaction

Xiaoyong Zhang,*[a] Pierre-Louis Lefebvre,[a,b] Jeremy N. Harvey*[a]

[a.] Theoretical and Computational Chemistry, Department of Chemistry, KU Leuven Celestijnenlaan 200F, 3001, Leuven, Belgium. E-mail: jeremy.harvey@kuleuven.be; zhangxyleuven@gmail.com

[b.] Quantum Theory Project, Departments of Chemistry and Physics, University of Florida, Gainesville, Florida 32611, United States

AUTHOR INFORMATION

Corresponding Author

Jeremy N. Harvey : jeremy.harvey@kuleuven.be

Xiaoyong Zhang : zhangxyleuven@gmail.com

ORCID

Xiaoyong Zhang : 0000-0002-0966-4343

Jeremy N. Harvey : 0000-0002-1728-1596

Abstract: How solvent motions affects the dynamics of chemical reactions in which the solute undergoes a substantial shape change is a fundamental but elusive issue. This work utilizes reactive simulation and Grote-Hynes theory to explore the effect of solvent motions on the dynamics of the Diels-Alder reaction (in the reverse direction, this reaction involves very substantial solute expansion) in aprotic solvents. Results reveal that the solvent environment is not sufficiently constraining to influence transition state passage dynamics, with the calculated transmission coefficients being close to unity. Even when solvent motions are suppressed or artificially slowed down, the solvent only affects the reaction dynamics in the transition state region to a very small extent. The only notable effect of solvent occurs far from the transition state region and corresponds to caging of the reactants within the reactant well.

TOC GRAPHIC

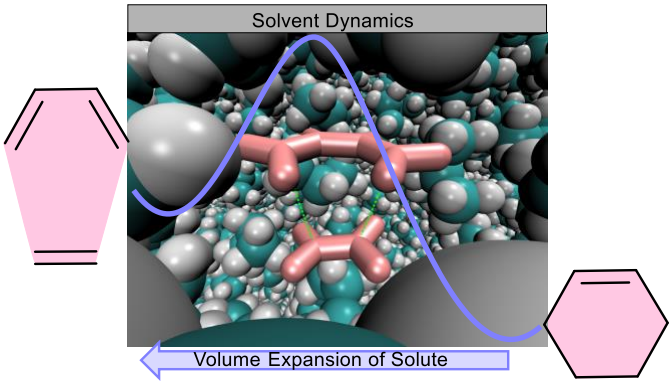

KEYWORDS : Solute Volume Expansion; Solvent Relaxation; TS passage dynamics; Grote-Hynes Theory; Empirical Valence Bond Simulation;

1. Introduction

Understanding how solvent regulates the kinetics and thermodynamics of chemical reactions is a fundamental and fascinating challenge, since most chemical and almost all biochemical reactions take place in solution.[1–7] Many solvent properties have been found to be important in affecting reactivity.[6] Computational chemistry combined with kinetic theories, such as transition state theory (TST), serves as one main technique to elucidate reaction mechanisms, and to quantify the reaction rate and product selectivity in solution phase.[8–10] In calculations, the solvent is treated either implicitly by structureless dielectric continuum models that respond to changes in solute polarity along the reaction pathway, or explicitly by atomistic models that account for specific solute-solvent interactions.

Nevertheless, most computational studies have been completed under the assumption of equilibrium solvation, in which solvent reorganization occurs instantaneously upon changes in the solute structure, so that the solvent adapts immediately as the reacting systems undergoes changes in its geometrical shape or its electron density distribution. In fact, as revealed by experimental and theoretical work,[11–15] solvent reorganization around a changing solute occurs on a finite timescale, typically of the order of several picoseconds, which is slower than the timescale on which chemical motion through the transition state region takes place (typically hundreds of femtoseconds), but is instead similar to the lifetime of some reactive intermediates, whose formation and disappearance can hence be influenced by the solvent dynamics.[16] The mismatch between solvent reorganization and reaction timescales could make the equilibrium solvation assumption inaccurate and hence invalidate its use when predicting reaction reactivity and selectivity.[17–21] Also, in this sort of instantaneous response picture, the dynamic flow of rovibrational energy that is known to occur during chemical reactions cannot be accounted for in terms of its truly dynamical effect on reactivity.[16,22–25] Instead, these dynamical effects regarding the motions of solute and solvent could be captured in trajectory-based dynamics simulations, .[26–30]

Due to the complexity of solvent-solute interactions, and the demanding computational resources associated with using quantum mechanics (QM)-based potentials, there are relatively few studies with well-converged sampling and realistic potential energy surfaces (PES) for reactions in solution. Ab initio molecular dynamics, and hybrid quantum mechanics and classical mechanics (QM/MM) simulations are widely used in such studies, but they are typically limited to picosecond timescale simulations, and are computationally prohibitive for extensive sampling of the phase space. The traditional MM force-field method, though computationally feasible, is unable to describe reactive events due to the fixed bonding topology associated with the force-field. Reactive MM methods that are able to treat bond breaking and formation, such as the empirical valence bond (EVB) method,[31–34] could serve as an alternative and economical choice for such computational tasks if carefully parameterized. Using the EVB surface means we have a fairly accurate and very computationally economical protocol for a 'real' reaction system, thus allowing for very extensive sampling and modelling of various solvent effects.

The picture emerging from existing computational studies of reaction dynamics in solution is influenced by the choice of the type of reaction studied. Many papers address reactions with peculiar potential energy surfaces with 'flat' regions and complex topologies[17,18,43–45,35–42] which usually involve multi-step reaction mechanism, and multiple distinct types of interactions between solute and solvent. These studies often show heavily "non-statistical" behaviour, in which the dynamical interactions between solute and solvent play a vital role in modulating the solute behaviour (including motions and energy partitioning) in the TS and post-TS regions, and altering the product selectivity.[40],[42] Some models, such as Kramers theory and Grote-Hynes theory developed to account for these deviations, suggest that non-standard behaviour might be very common in solution-phase reactions.[10,45–49] One practical way to account for the non-equilibrium solvation effect during the calculation of reaction rate is to compute the transmission coefficient as a correction of the TST rate constant.

There have been fewer studies of more standard chemical reactions involving significant transition state barriers, even though many of these reactions have prima facie potential for involving significant coupling to solvent due e.g. to major changes in solute volume along the reaction coordinate. The more general topic of solute volume changes has been studied, but mostly using simple model systems.[50–53] Schwartz and coworkers compared the solvent relaxation dynamics triggered by changes in solute size for a Lennard-Jones sphere in water.[50,51] As a response to solute volume expansion, solvent has to take some time to reorganize itself, especially the first solvation shell solvent molecules would be driven to move outwards into the second shell. Slow solvent motion, as compared to the timescale of the solute shape changes, could thus induce transient strong solvent-solute interactions, with the reaction progress (involving volume change of the solute) needing to "wait" for solvent movement, thereby creating an extra "inertial" barrier to reaction. This dynamical blocking phenomenon, associated with the solvent motions triggered by the solute expansion, is thus different with, and could not be accounted for by the solvent frictional (viscosity) effect affecting solute motions as addressed in the widely-adopted Kramers theory and the generalized Grote-Hynes theory.[46] Carpenter recently introduced a related simple physical model to stress the effect of solute shape changes on reactivity in nonpolar systems,[52],[53] with the bath or solvent being represented by a single one-dimensional harmonic oscillator term, which interacts with the solute through a Lennard-Jones type repulsive term $(r_2 - r_1)^{-12}$. The solute reactivity is described by a double-well potential. Using this model, it was predicted that simply by changing solvent mass, the position of the dynamical dividing surface to reaction (the surface through which no recrossing events occur) can be altered to lie far away from the saddle point of the solute potential energy surface. In other words, the transmission behaviour of trajectories across the TS saddle point could be significantly altered. Thus, the authors suggested conventional transition state theory might be inadequate to predict the reaction rate constants for reactions with substantial solute shape expansion.

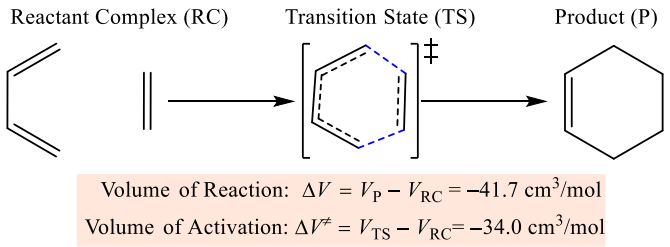

Scheme 1. Diels-Alder reaction of ethene and butadiene. Values of volume of activation and reaction were extracted from reference 54.

Here we study a paradigmatic solution-phase organic reaction, the Diels-Alder (DA) reaction (**Scheme 1**) in aprotic solvent (propane), and attempt to clarify the solvent effect associated with substantial change in solute shape from reactant to product. Solvent-reactant interactions are non-polar in this system, so that polar solvation effects are negligible in influencing the structures of the transition state. Nevertheless, the change in system volume as it passes through the TS region is important, as indicated by the very negative (−34.0 cm^3/mol) volume of activation ($\Delta V^{\ddagger}$) that was calculated for the reaction.[54–56] Correspondingly, the solute volume expands significantly along the reaction coordinate when considering the reverse reaction, i.e. the so-called retro-Diels Alder reaction. While the experimental $\Delta V^{\ddagger}$ is not available for the parent reaction, it has been measured for similar Diels-Alder reactions, and experimental and computational results for those cases generally agree quite well.[55] Therefore, this reaction provides a good test of various "caging" and "dynamical blocking" effects, and those proposed theoretical models. In addition, in our computational study, the magnitude of solvent inertial effects can be alchemically probed by varying the solvent mass. On the other hand, the potential energy surface for this reaction has a fairly sharp maximum along the reaction coordinate corresponding to the transition state, so major dynamical effects other than those associated with solvent coupling are not expected.

2. Computational Details

DFT Calculations. The reactive potential energy surface of the DA reaction was mapped with a two-dimensional scan varying the two reacting C—C distances R_{ac} and R_{bd} (**Scheme 2**) from 1.5 Å

to 3.6 Å in steps of 0.1 Å, with all other coordinates optimized. For regions of the potential energy surface with one short reactive C—C bond and one long one, a diradical electronic structure is possible, hence careful tests were carried out in order to identify whether unrestricted Kohn-Sham solutions existed. Structural optimizations were conducted at the M06-2X/6-31G(d) level with the Gaussian 16 program package,[57] and the energies were further re-fined at the M06-2X/6-311+G(d,p) level.

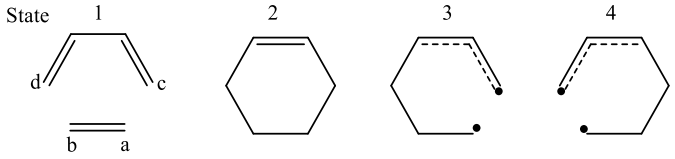

Scheme 2. The four diabatic states in the EVB matrix.

EVB Simulations. A four-state EVB Hamiltonian was developed to model the reactive events in the DA reaction (eqs. 1-4).

$$H = \begin{bmatrix} H_{11}+\varepsilon_1 & H_{12} & 0 & 0 \\ H_{21} & H_{22}+\varepsilon_2 & H_{23} & H_{24} \\ 0 & H_{32} & H_{33}+\varepsilon_3 & 0 \\ 0 & H_{42} & 0 & H_{44}+\varepsilon_4 \end{bmatrix} \quad (1)$$

$$H_{12} = H_{21} = A_{12}\exp\left(-\frac{1}{2}\left(\frac{R_{ac}+R_{bd}-r_{12}^0}{\sigma_{12}}\right)^2\right) \quad (2)$$

$$H_{23} = H_{32} = A_{23}\exp\left(-\frac{1}{2}\left(\frac{(R_{ac}-R_{bd})-r_{23}^0}{\sigma_{23}}\right)^2\right) \quad (3)$$

$$H_{24} = H_{42} = A_{24}\exp\left(-\frac{1}{2}\left(\frac{(R_{bd}-R_{ac})-r_{24}^0}{\sigma_{24}}\right)^2\right) \quad (4)$$

In the equation, H_{11} and H_{22} are single-state MM energies computed for the system using the bond connectivity of the reactants and the product respectively, while H_{33} and H_{44} denote MM single-state energies of each of the two diradical states (**Scheme 2**). The off-diagonal H_{ij} $(i \neq j)$ terms of equations (2 - 4) are one-dimensional Gaussian functions that determine the coupling strength between the different EVB states, with parameters (A, r^0, σ) chosen to fit the M06-2X energies (ESI). The ε_i values are shift terms that ensure the correct reaction energies. The MM3[58–60] force

field was used to compute the inter-/intra-molecular interactions in each EVB state. EVB type calculations and simulations were conducted with our in-house MPI-parallelized EVB code[61] adapted within Tinker 8 software.[62]

The simulation system was built with 53 propane molecules and the reactive species in a box of 20.0 Å, to reproduce the density of liquid propane (0.493 g/cm^3) at room temperature. The free energy change near the transition state along the reaction coordinate was derived from the potential of mean force (PMF) simulations by using umbrella sampling[63] together with the weighted histogram analysis method (WHAM),[64] with reaction coordinate $q_{RC} = R_{ac} + R_{bd}$.[30,65,66] Seventeen separate harmonic umbrella sampling potentials were used, centred at values of q_{RC} between 4.40 Å and 4.56 Å in steps of 0.01 Å, with a force constant of 1300 kcal/mol/Å^2. For each window, a 2 ns equilibration step was followed by a 6 ns production phase, in each case using a 1 fs timestep, the NVT ensemble (using the Bussi algorithm[67]) at 300 K, and the velocity Verlet algorithm.[68] vdW interactions were switched from 8 Å and fully truncated at 9 Å.

We found that the π-electron SCF component of the MM3 force field displayed poor convergence for some distorted structures during the solution-phase dynamics, leading to poor energy conservation and trajectory failure. Problematic behaviour of this type can be detected by monitoring the C—C—C—C dihedral angle of the butadiene fragment (values above 90° exacerbate the problem) as well as the number of SCF iterations required for convergence during the simulations (**Table S3**). A similar problem has been noted previously.[69] The problem can be essentially removed, certainly in the TS region that is important for this study, by increasing the mass of all hydrogen atoms within the reactive system to three times their normal mass, leading to slightly slower motions for the (in any case stiff and roughly adiabatic) hydrogen atoms and better convergence of the π-electron SCF procedure.

For the rare event trajectory simulations, a 2.6 ns equilibration simulation was conducted in the NVT ensemble, with q_{RC} constrained by the *Rattle* algorithm[70] at the maximum of the PMF, with 600 snapshots randomly selected from the final 0.6 ns. For each snapshot, the velocity along the reaction coordinate was altered so that overall the kinetic energy in this mode followed a Boltzmann distribution with T = 300 K.[71],[72] Downhill trajectories were obtained by propagating each sampled snapshot both forward and backward (reversing the velocity of the reaction coordinate) for 400 fs with a time step of 0.1 fs in the NVE ensemble.

The time-dependent transmission coefficient could be determined from the trajectories by using the reactive flux method[72] (eqn. 5—7).

$$k(t) = \frac{\left\langle \dot{q}_{RC}(t=0)\theta\left(q_{RC}(t) - q_{RC}^{\ddagger}\right)\right\rangle_{q_{RC}^{\ddagger}}}{\frac{1}{2}\left\langle \left|\dot{q}_{RC}(t=0)\right|\right\rangle_{q_{RC}^{\ddagger}}} \tag{5}$$

$$q_{RC}^{\neq} = R_{ab}^{\ddagger} + R_{cd}^{\ddagger} \tag{6}$$

$$\theta\left(q_{RC}(t) - q_{rc}^{\ddagger}\right) = \begin{cases} 0; & q_{rc}(t) \leq q_{rc}^{\ddagger}; \text{ the DA product region} \\ 1; & q_{rc}(t) > q_{rc}^{\ddagger}; \text{ the DA reactant region} \end{cases} \tag{7}$$

In the equation, $\theta(q_{RC}(t) - q_{RC}^{\ddagger})$ is the Heaviside step function, $q_{rc}^{\ddagger}$ is the reaction coordinate value at the maximum of PMF, and $q_{RC}(t)$ is the time-dependent reaction coordinate value. The trajectories are initiated at $q_{RC}^{\ddagger}$ such that $q_{RC}(t=0) = q_{RC}^{\ddagger}$. $\dot{q}_{rc}(t=0)$ is the internal coordinate velocity of the reaction coordinate at the PMF top ($t=0$). The initial velocities for all other coordinates were taken from long constrained dynamics simulations, while the initial velocity $\dot{q}_{RC}(t=0)$ is randomly sampled from a Boltzmann distribution, with average value k_bT. For the simulations performed using non-standard masses for the solvent atoms, velocities were sampled from constrained dynamics carried out using the appropriate solvent masses, while the same set of random values of $\dot{q}_{RC}(t=0)$ as for the parent standard mass simulations were used. $\langle \ldots \rangle_{q_{RC}^{\ddagger}}$ represents an ensemble average over the 600 trajectories sampled with the reaction coordinate constrained at the PMF saddle point. A typical $k(t)$ curve is featured with a short-time decay

process associated with any recrossing events, and once all the trajectories reach the reactant or product state, $k(t)$ then presents a plateau corresponding to the transmission coefficient.

Grote-Hynes theory. Grote-Hynes (GH) theory[47] is one of the rate theories to derive rate constants, and has been successfully used to estimate the transmission coefficient of reactions in solutions and enzymes.[73],[74] GH utilizes the linear generalized Langevin equation (GLE) to describe the dynamics of the reaction coordinate in the TS region, with the effect of the remaining degrees of freedom (solvent and nonreactive solute motions) introduced through the equilibrium forces and dynamical friction forces that they exert on the reaction coordinate. In the vicinity of the barrier top, the transmission coefficient (refer to GH value) is simply obtained as the ratio of the so-called reactive frequency ω_r and the so-called equilibrium frequency $\omega_{b.eq}$.

$$\kappa_{GH} = \frac{\omega_r}{\omega_{b.eq}} \tag{8}$$

The equilibrium frequency $\omega_{b.eq}$ is defined based on the magnitude of the curvature (k_{PMF}) of the potential of mean force (PMF) curve U_{PMF}. This PMF curve can be computed using a variety of methods, but always assuming equilibrium solvation.

$$\Delta U_{PMF} = -\frac{1}{2} k_{PMF} \left(q_{RC} - q_{RC}^{\ddagger}\right)^2 \tag{10}$$

$$\omega_{b.eq} = \frac{1}{2\pi c} \sqrt{\frac{k_{PMF}}{\mu}} \tag{11}$$

in which ΔU_{PMF} is the difference between the PMF value at a given value of the reaction coordinate q_{RC} and the PMF value at the maximum $q_{RC}^{\ddagger}$, while μ is the reduced mass associated with the reaction coordinate.

The reactive frequency ω_r, which is related with the time scale for reaction coordinate motions at the barrier top, can be computed by solving the eqn (12).

$$\omega_r^2 - \omega_{b,eq}^2 + \omega_r \hat{\zeta}(\omega_r) = 0 \tag{12}$$

$$\hat{\zeta}(\omega_r) = \int_0^\infty \zeta(t) e^{-\omega_r t}\, \mathrm{d}t \tag{13}$$

$$\zeta(t) = \frac{\langle F(0)F(t)\rangle}{\mu k_B T} \tag{14}$$

where $\hat{\zeta}(\omega_r)$ is the Laplace transform of the time-dependent friction kernel $\zeta(t)$ at the reactive frequency ω_r. $\zeta(t)$ is proportional to the autocorrelation function of the forces ($F(t)$) that act on the reaction coordinate, T is the temperature (300 K), and k_B is the Boltzmann constant. In the absence of friction, so in the case where $\zeta(t)$ is zero and one always has equilibrium solvation with solvent fully equilibrated to changes in the reaction coordinate at all times, the rate of change of the reaction coordinate within the barrier region is determined by the negative derivative of the PMF, and the reactive frequency ω_r is then equal to the equilibrium frequency $\omega_{b.eq}$. In the presence of non-zero friction (non-equilibrium solvation), motion along the reaction coordinate can be impeded by 'collisions' with the solvent molecules (or more generally the atoms in the environment) which usually leads to slower motion than would be caused purely by the PMF. This also leads to solvent-induced barrier recrossing. That means, the reaction time scale (ω_r^{-1}) in the presence of non-equilibrium solvation depends on both the equilibrium frequency $\omega_{b.eq}$ and the solvent dynamics, with the latter being introduced into the above equation and into GH theory through the friction kernel $\zeta(t)$. As a result of the barrier recrossing and the reduced net rate of passage across the barrier region, ω_r is smaller than $\omega_{b.eq}$ and hence the transmission coefficient $\kappa_{GH}$is smaller than 1.

Solving the GH equation requires the determination of the PMF curve (already known from the free energy calculations), and calculations of the friction kernel $\zeta(t)$ from a constrained MD simulation with the reaction coordinate constrained at the maximum of the PMF. To get the friction kernel, 40 ps NVE simulations were performed using a time step of 0.05 fs. In the simulation, the reaction coordinate was constrained by the Rattle algorithm, and the forces on the reaction coordinate were collected every time step. The Wilson matrix was used to convert internal velocity and Cartesian velocity.

It is important to mention one limiting case of GH theory, the nonadiabatic regime, where reaction is much faster than environment responses. The reaction time scale is so short that solvent has no time to respond. Therefore, the solvent can be treated as frozen (no solvent dynamics) during the TS passage, and it is the initial configuration (*i.e.*, the zero-time value of the friction kernel $\zeta(t) = \zeta(t = 0)$) that plays a role in affecting the reactive frequency ($\omega_{b,na}$). In this case, $\hat{\zeta}(\omega_r)$ reduces to $\omega_r^{-1}\zeta(t = 0)$, and eqn (12) becomes,

$$\omega_{b,na}^2 = \omega_{b,eq}^2 - \zeta(t = 0) \tag{15}$$

3. Discussions

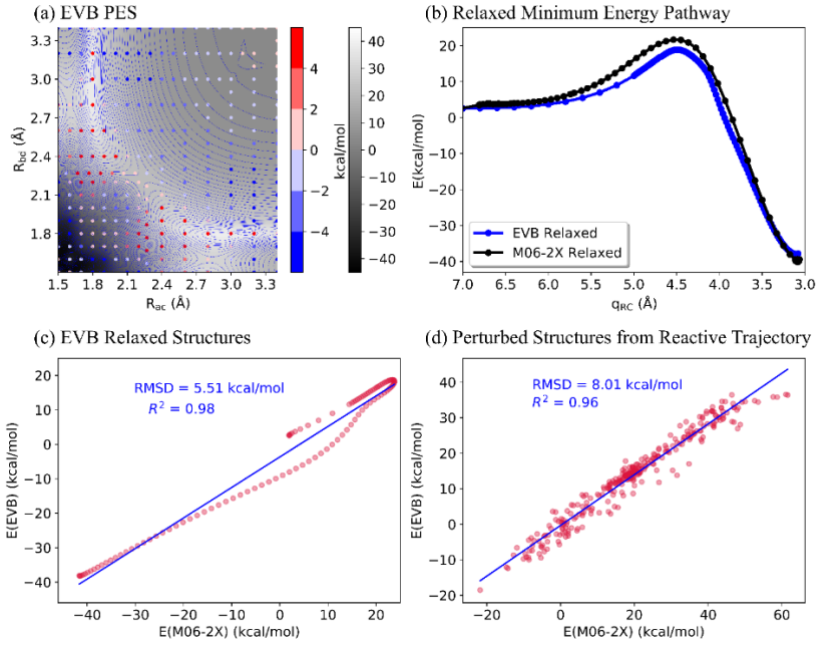

Figure 1. (a) Contour plot of the reactive four-state EVB PES for the symmetric DA reactions. The colored dots signal the difference between the energies predicted at each point by EVB and M06-2X, with blue dots indicating points where the EVB relative energy is lower than the DFT one, and red dots indicating the reverse. (b) Relaxed minimum energy reaction pathway along the reaction coordinate as predicted by the multistate EVB potential (in blue) and M06-2X method (in black). (c) and (d) correlation of the single point energy predicted by EVB and M06-2X for structures extracted (c) from EVB relaxed scan, and (d) from the EVB reactive dynamics. The least-squares regression lines are shown in blue.

A reactive four-state empirical valence bond (EVB) potential energy surface (PES), that is capable to model the Diels-Alder (DA) reaction in solution, was firstly parameterized. Fitting results in an EVB potential (**Figure 1a**) with a root mean square deviation (RMSD) of 4.6 kcal/mol (R^2 =0.95) from the DFT energies for the 317 structures, corresponding to a two-dimensional relaxed scan at the M06-2X level of theory (**Figure S1**). For the subset of 160 relaxed scan structures that are within 0.5 Å of the diagonal line $R_{ac} = R_{bd}$, the agreement between EVB and DFT is somewhat better, with an RMSD of 2.2 kcal/mol. Additional M06-2X single point energy calculations on 107 structures along the EVB-relaxed minimum energy pathway yield an RMSD of 5.5 kcal/mol and R^2 of 0.98 (**Figure 1c**). A further 300 structures were randomly sampled from the reactive trajectories in solution phase. Over these structures, the correlation between EVB energies and *ab initio* energies is very good (R^2 = 0.96 in **Figure 1d**), but the deviation between the EVB energies and the M06-2X energies is relatively large (RMSD = 8.0 kcal/mol). The large RMSD is traced to the difference between the MM3 force field and the M06-2X functional in describing the degree of freedoms orthogonal to the reaction coordinate. Overall, the current EVB PES preserved the performance of DFT (M06-2X) in describing the reaction profile and geometry along the reaction coordinate of the DA reaction (**Figure 1b** and **S2**).

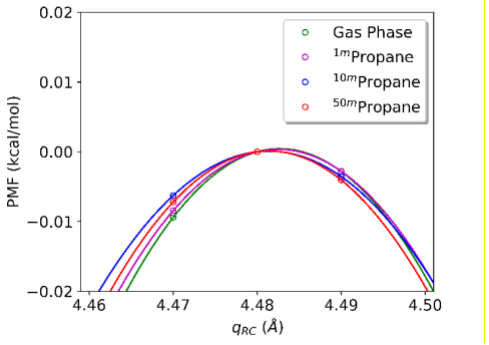

Figure 2. Potential of mean force in the vicinity of the barrier top in the gas phase and in solutions with varying solvent mass.

Then, we moved to study the DA reaction dynamics in solution by using the reactive EVB potential. The aprotic and non-polar propane is chosen as the solvent, so that we only consider the effect of non-electrostatic interactions between solvent and solute. In this paper, to avoid confusion, the term "solvent" is used to refer to all the propane molecules in the system, whereas the term "environment" refers to all non-reactive degrees of freedom, including the coordinates of the solvent atoms, as well as the solute intramolecular modes. To assess the effect of solvent mass on the position of the transition state of the DA reaction in solution, we mapped the free energy profile of the reaction near the barrier top in the gas phase and solvents of varying masses (**Figure 2**). Our results show that the PMF of the Diels-Alder reaction is not very much influenced by the solvent in the TS region. The position of the maximum of the PMF, obtained by fitting the curve to parabolic functions, is nearly invariant (~4.815 Å) on increasing the solvent mass from the standard value (^{1m}Propane) to 50 times the standard one (^{50m}Propane). The changes in shape of the PMF upon moving from the gas phase to solution and changing the solvent atom masses are similar in magnitude to the statistical error (~0.001 kcal/mol) in the PMF estimated from the WHAM analysis. The current observation with a more realistic description of solvent-solvent interaction, points out that weakly-interacting solvent has a minor effect on modifying the free energy surface for a typical organic reaction, even with substantial shape changes along the reaction coordinate.

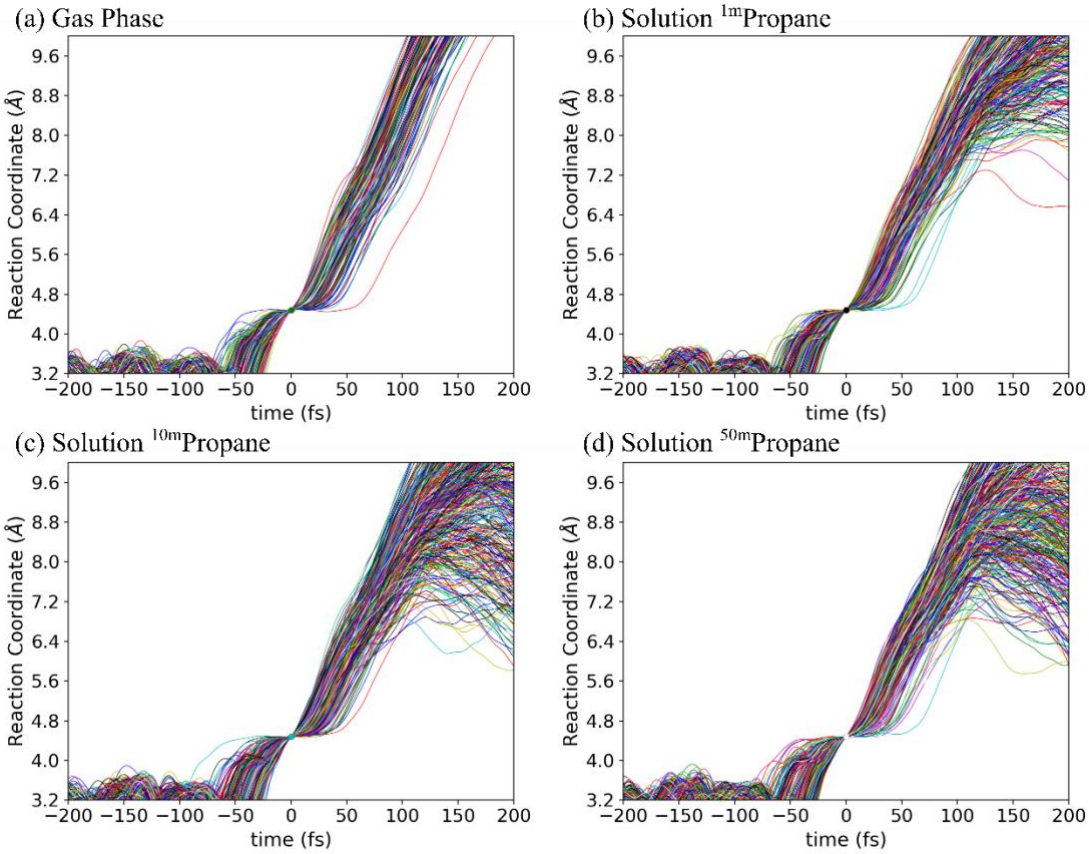

Figure 3. Time evolution of the reaction coordinate in reactive trajectories of the DA reaction in the gas phase and in solution with different solvent masses, as predicted by the four-state EVB potential. The system lies within the dividing surface (reaction coordinate equal to its value at the peak of the PMF) at time zero; positive time corresponds to the trajectory moving to the reactant side while negative time corresponds to the product side.

Initialized from a set of sampled snapshots in the transition state region, the reaction dynamics were studied by using the downhill dynamics simulation strategy.[73] For each system in the gas phase or in solution, 600 trajectories were run, and each trajectory was propagated forward and backward, in each case for a time sufficient for either the product (q_{RC} < 3.4 Å) or the reactants (q_{RC} > 5.8 Å) to be formed, with the two half-trajectories then combined to form an overall trajectory. These can then be divided into two classes, reactive trajectories (which go from reactants to product), and non-reactive trajectories (which go from reactants to reactants, or from product to product). The proportion of non-reactive trajectories slightly increases from the gas phase reaction (38 out of 600) to the various solvent media, and using a heavier solvent also leads to a slightly

increased fraction of non-reactive trajectories (**Table S2**). Nevertheless, these differences are small and overall, the dynamics of passage through the TS saddle point is barely modified by the solvent, compared to the gas phase (**Figure 3**). Transition from the saddle point structure towards the product or reactants well occurs rapidly, typically within ~50 fs. At longer times in the dynamics, a feature that can be observed for solution trajectories entering the reactant region, but that is absent in those performed in the gas phase, is the solvent caging effect, whereby the separation between the reactants (butadiene and ethene) ceases to increase at some point. However, this caging effect occurs only upon fully entering the reactants well for values of the reaction coordinate larger than ~6.5 Å. The degree of caging is as expected somewhat stronger in the heavier solvent, which witnesses more trajectories reversing the velocity of the reaction coordinate due to the slower motions of solvent and more frequent solute collisions with the solvent.

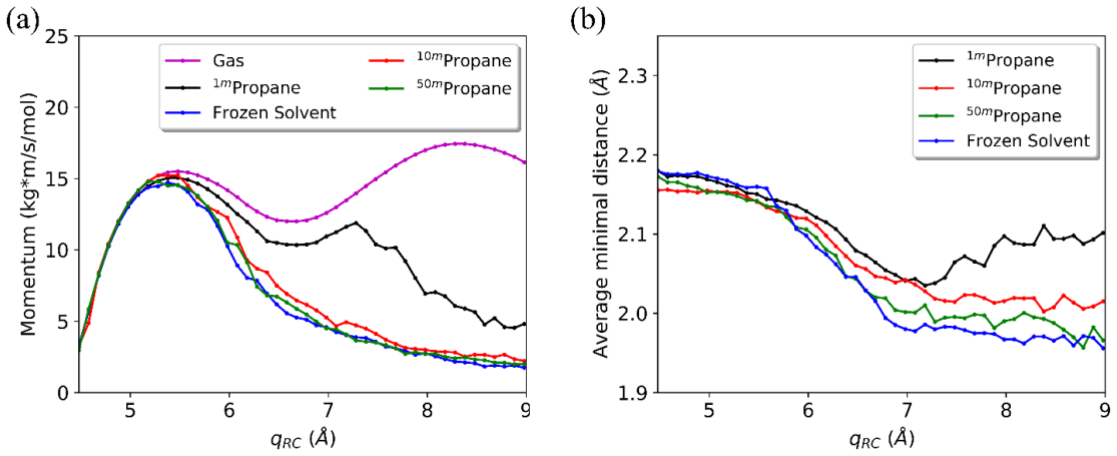

Figure 4. (a) Average momentum of the reaction coordinate in the direction leading to reactant complex in different simulation systems over all reactive trajectories; (b) The shortest solvent atom – solute atom distance along the reaction coordinate in different simulation systems averaged over all reactive trajectories.

Another way to illustrate the modest effect of solvent on dynamics in the region surrounding the TS is to plot the average momentum along the reaction coordinate and the average of the shortest distances between a solute atom and a solvent atom (average over all trajectories) as a function of

the reaction coordinate (**Figure 4**) for all trajectories. In the gas phase, after exiting the transition state region, the reaction coordinate continuously accelerates until reaching a value near 5.5 Å owing to the decrease in potential energy (**Figure 1b**). Beyond that distance, the system has entered the flat reactants well, and there will be some extent of interchange between kinetic energy and potential energy, accounting for the oscillation of the momentum. In solvents of varying mass, the evolution of the average momentum is almost identical for values of the reaction coordinate up to ~5.5 Å, with caging effects then becoming more important. As can be seen, the trajectories in the reactant region also involve closer average solvent-solute distances (**Figure 4b**) because the solvent cage has not yet responded to the volume expansion of the solute, at least during the simulated timescale (400 fs) of the trajectories.

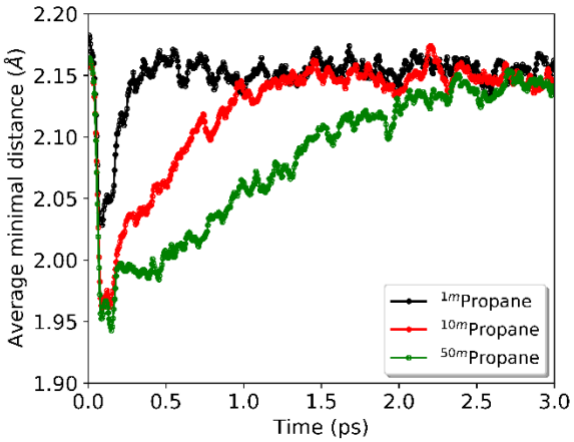

Figure 5. Average of the shortest solvent atom - solute atom distance during 400 reactive trajectories headed towards reactants.

Activated chemical reactions require accumulation of energy within the reactant sub-system prior to barrier-crossing, and its dissipation after crossing the barrier. Experimental and computational studies show that this energy exchange occurs more slowly than bond making and breaking, on a timescale of the order of a few ps to a few tens of ps.[37,59–61] The present reaction is an example of a process with a significant activation *volume*, and the present simulations provide an indication of

the relative timing of the volume change and of the bond-making and breaking events. Over the 400 fs timescale of the main reactive simulations, starting from the more compact TS, the trajectories entering the reactants region do not fully allow expansion of the solvent cage. Extending these simulations to longer time (**Figure 5**) shows solvent expansion (as measured by minimum solute-solvent distance) with a time constant of roughly 0.14 ps in ^{1m}Propane, 0.55 ps in ^{10m}Propane and 1.32 ps in ^{50m}Propane, tending towards a minimum distance equal to that found in equilibrium simulation of the reactants, which is of 2.16 Å, very similar to that found for the TS. Based on this, and considering now the reaction in the forward direction from reactants to product, it appears that volume fluctuations behave similarly to energy fluctuations, with the actual reactive event occurring only for those structures with high solvent density around the reactants.

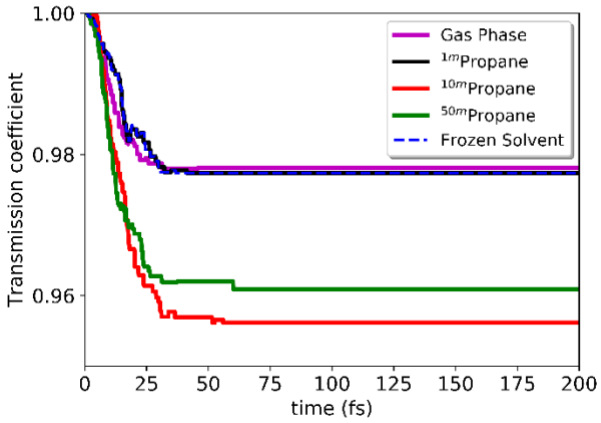

Figure 6. Time-dependent transmission coefficient reaction in gas phase and solution of varying solvent mass. The case with all standard mass solvent molecules frozen in the dynamics is shown by the blue dashed line.

Then, the time-dependent transmission coefficients were calculated from the trajectories (**Figure 6**). All reaction systems show a rapid decay in the transmission coefficient within the first 25 fs, which is caused by a small number of trajectories exhibiting recrossing behaviour (**Figure S6**) while still within the TS region. A plateau is then reached indicating that very few recrossing events occur once the system has moved out of the immediate TS, and the overall transmission coefficient can hence be obtained. Nearly identical decay behaviour was found for the reaction in the gas phase

and ^{1m}Proprane. The transmission coefficients are both close to 0.98 and thereby near to the TST limit. Thus, propane of normal mass shows only a very small effect on trajectory recrossing, such that solvent motion is only weakly coupled to the reaction coordinate and the solvent friction effect is very small. The fact that the transmission coefficient is close to unity also indicates that the sum of the two bond lengths is a good approximation of the reaction coordinate for the symmetric DA reaction.[53,78] By changing the solvent mass to a heavier one (^{10m}Propane and ^{50m}Propane), the transmission coefficient only decreases slightly, to ~0.96 , suggesting that solvent mass change only has a modest effect on transition state passage dynamics.

An even more drastic way to model the possible extent of solvent constraints on the reaction dynamics is to treat solvent as being completely frozen, at the sampled saddle-point structures used to initiate dynamics. Under this limit, essentially no change occurs in the transmission behaviour (**Figure 6**) with respect to the trajectories with mobile solvent, indicating that the solvent cage does not effectively impact upon the TS dynamics. The small changes in the time-dependent transmission coefficient reflect instead small changes in the initial value of the reaction coordinate, taken in each case as the value at the maximum of the PMF for the corresponding solvent mass. Indeed, this effect, rather than a greater solvent friction, likely accounts for the small changes in transmission coefficient noted above for the heavy solvent cases.

The dynamic effect of solvent mass changes on reaction rate is further evaluated by Grote-Hynes (GH) theory, which derives the transmission coefficient as the ratio of the reactive frequency (ω_r, the reaction time scale) and equilibrium frequency ($\omega_{b,eq}$, the magnitude of the curvature at the PMF top). The ω_r determined from GH theory is 598.0, 603.9 and 593.43 cm^{-1} (**Table 1**) for reaction in the standard solvent, 10 times and 50 times mass solvents, which indicates that reaction has a comparable reaction time scale ($1/(2\pi\omega_r)$, ~9 fs) in these three systems. As a comparison, the environment relaxation time scale, as determined as the ratio of the friction constant and zero-

time friction kernel, is a bit larger (~20 fs for the standard solvent system) than the reaction time scale, but of the same magnitude, indicating again only modest solvent effects.

Table 1. Equilibrium frequency, reactive frequency ω_r and transmission coefficient obtained from Grote-Hynes theory κ_{GH} and its non-adiabatic limit κ_{NA}.

	ω_r (cm^{-1})	$\omega_{b,eq}$(cm^{-1})	κ_{GH}	κ_{NA}
G[a]	646.5	693.3	0.93	0.80
^{1m}Propane	598.0	664.0	0.90	0.66
^{10m}Propane	603.9	642.5	0.94	0.80
^{50m}Propane	593.4	665.3	0.89	0.62

The transmission coefficient computed by GH theory is comparable for reactions in lighter and heavier solvents, in agreement with what we obtained from the trajectory simulations. The transmission coefficient from GH theory (0.89-0.94) is slightly smaller than those obtained from the rate event trajectories, but still very close to unity, and again suggests that friction effects from solvent and the remaining degree of freedoms of solute are small in the immediate TS region. In addition, the current results also show that GH theory is a reliable method to estimate the transmission coefficient for the DA reaction in solution. The transmission coefficient obtained within GH theory assuming the limiting frozen environment regime (i.e. with no motion of the solvent or of the 'spectator' degrees of freedom within the solute), is 0.66-0.80, somewhat more distant from unity, suggesting that motion within the remaining 'spectator' degrees of freedom within the reacting molecules is dynamically coupled to the reaction coordinate, influencing the recrossing event, since direct simulations (**Figure 6** and **S4**) with frozen solvents show little change in the transmission coefficient.

4. Conclusion

In this work, we present a detailed study on the reaction dynamics and solvent relaxation dynamics associated with solute volume expansion in non-polar solvent for a typical activated chemical reaction, the Diels-Alder reaction. Extensive sampling of the solvent motion during reaction could be performed at low computational cost thanks to the efficiency of the adopted

empirical valence bond potential, parameterized based on quantum chemical computations. Both the trajectory simulations and Grote-Hynes theory calculations revealed the transmission coefficient to be close to unity in solution, even in the artificial case where solvent relaxation is slow (imposed by increasing the solvent mass) or even completely frozen. These findings here, by using a realistic atomic system, contrast with the predictions of a previously proposed theoretical model,[52,53] which predicted that solvent motions could significantly alter the transition state behaviour for reactions with substantial solute volume expansion. This low-dimensional model simply treats solvent as a "wall" that directly couples to reaction, and thus, apparently overstates coupling.

Solvent motions do indeed have an effect during the volume expansion of the solute, but this effect only materializes at very large values of the reaction coordinate, at the point at which diffusion of the two reactants away from each other starts to occur. This effect is therefore best described as solvent-induced impedance of the separation of reactant species, i.e., the caging effect, instead of hindrance for TS crossing, which in this system at least is found to be a very modest effect. As mentioned earlier, this observation contrasts with other dynamics-based studies in which a significant impact of solvent on reaction outcomes has been observed.[16–18,23,25,40,42–45] In some of those cases,[16,25] the effect is due to non-thermalized and short-lived intermediates, which are not present here. For the almost entirely non-bonded and non-polar effects that can occur here, solvent motions have a minor effect on transition state passage.

Acknowledgements

Xiaoyong Zhang appreciates the China Scholarship Council (CSC) for providing a doctoral scholarship. The computational resources and services used in this work are provided by the VSC (Flemish Supercomputer Center), funded by the Research Foundation-Flanders (FWO) and the Flemish Government-department EWI.

References

[1] M. Orozco, F. J. Luque, *Chem. Rev.* **2000**, *100*, 4187–4226.

[2] A. J. Orr-Ewing, *Chem. Soc. Rev.* **2017**, *46*, 7597–7614.

[3] M. A. Mellmer, C. Sanpitakseree, B. Demir, P. Bai, K. Ma, M. Neurock, J. A. Dumesic, *Nat. Catal.* **2018**, *1*, 199–207.

[4] Z. Zhao, R. Bababrik, W. Xue, Y. Li, N. M. Briggs, D. T. Nguyen, U. Nguyen, S. P. Crossley, S. Wang, B. Wang, et al., *Nat. Catal.* **2019**, *2*, 431–436.

[5] L. R. Pestana, H. Hao, T. Head-Gordon, *Nano Lett.* **2020**, *20*, 606–611.

[6] C. Reichardt, T. Welton, in *Solvents Solvent Eff. Org. Chem.*, John Wiley & Sons, **2010**, pp. 165–357.

[7] W. J. Glover, R. E. Larsen, B. J. Schwartz, *J. Phys. Chem. Lett.* **2010**, *1*, 165–169.

[8] G. J. Cheng, X. Zhang, L. W. Chung, L. Xu, Y. D. Wu, *J. Am. Chem. Soc.* **2015**, *137*, 1706–1725.

[9] J. Gao, *Acc. Chem. Res.* **1996**, *29*, 298–305.

[10] J. L. Bao, D. G. Truhlar, *Chem. Soc. Rev.* **2017**, *46*, 7548–7596.

[11] A. Rosspeintner, B. Lang, E. Vauthey, *Annu. Rev. Phys. Chem.* **2013**, *64*, 247–271.

[12] J. Ma, D. Vanden Bout, M. Berg, *J. Chem. Phys.* **1995**, *103*, 9146–9160.

[13] M. Berg, *J. Phys. Chem. A* **1998**, *102*, 17–30.

[14] R. Rey, J. T. Hynes, *J. Phys. Chem. B* **2020**, *124*, 7668–7681.

[15] M. J. Bedard-Hearn, R. E. Larsen, B. J. Schwartz, *J. Phys. Chem. B* **2003**, *107*, 14464–14475.

[16] B. K. Carpenter, J. N. Harvey, A. J. Orr-Ewing, *J. Am. Chem. Soc.* **2016**, *138*, 4695–4705.

[17] Y. Nieves-Quinones, D. A. Singleton, *J. Am. Chem. Soc.* **2016**, *138*, 15167–15176.

[18] Z. Chen, Y. Nieves-Quinones, J. R. Waas, D. A. Singleton, *J. Am. Chem. Soc.* **2014**, *136*, 13122–13125.

[19] P. L. Geissler, C. Dellago, D. Chandler, *J. Phys. Chem. B* **1999**, *103*, 3706–3710.

[20] X. Hu, W. L. Hase, *J. Phys. Chem.* **1992**, *96*, 7535–7546.

[21] G. H. Peslherbe, R. Bianco, J. T. Hynes, B. M. Ladanyi, *J. Chem. Soc. - Faraday Trans.* **1997**, *93*, 977–988.

[22] D. R. Glowacki, C. H. Liang, S. P. Marsden, J. N. Harvey, M. J. Pilling, *J. Am. Chem. Soc.* **2010**, *132*, 13621–13623.

[23] H. Kurouchi, D. A. Singleton, *Nat. Chem.* **2018**, *10*, 237–241.

[24] B. K. Carpenter, *Chem. Rev.* **2013**, *113*, 7265–7286.

[25] H. Kurouchi, I. L. Andujar-De Sanctis, D. A. Singleton, *J. Am. Chem. Soc.* **2016**, *138*, 14534–14537.

[26] M. N. Grayson, Z. Yang, K. N. Houk, *J. Am. Chem. Soc.* **2017**, *139*, 7717–7720.

[27] Z. Yang, S. Yang, P. Yu, Y. Li, C. Doubleday, J. Park, A. Patel, B. sun Jeon, W. K. Russell, H. wen Liu, et al., *Proc. Natl. Acad. Sci. U. S. A.* **2018**, *115*, E848–E855.

[28] Z. Yang, C. Doubleday, K. N. Houk, *J. Chem. Theory Comput.* **2015**, *11*, 5606–5612.

[29] Y. Fu, L. Bernasconi, P. Liu, *J. Am. Chem. Soc.* **2021**, *143*, 1577–1589.

[30] J. Chandrasekhar, S. Shariffskul, W. L. Jorgensen, *J. Phys. Chem. B* **2002**, *106*, 8078–8085.

[31] K. V. Nelson, I. Benjamin, *Chem. Phys. Lett.* **2010**, *492*, 220–225.

[32] A. Warshel, R. M. Weiss, *J. Am. Chem. Soc.* **1980**, *102*, 6218–6226.

[33] S. C. L. Kamerlin, A. Warshel, *WIREs Comput. Mol. Sci.* **2011**, *1*, 30–45.

[34] C. Knight, G. A. Voth, *Acc. Chem. Res.* **2012**, *45*, 101–109.

[35] Z. Yang, C. S. Jamieson, X. S. Xue, M. Garcia-Borràs, T. Benton, X. Dong, F. Liu, K. N. Houk, *Trends Chem.* **2019**, *1*, 22–34.

[36] S. R. Hare, A. Li, D. J. Tantillo, *Chem. Sci.* **2018**, *9*, 8937–8945.

[37] D. R. Glowacki, R. A. Rose, S. J. Greaves, A. J. Orr-Ewing, J. N. Harvey, *Nat. Chem.* **2011**, *3*, 850–855.

[38] S. R. Hare, D. J. Tantillo, *Pure Appl. Chem.* **2017**, *89*, 679–698.

[39] B. R. Ussing, C. Hang, D. A. Singleton, *J. Am. Chem. Soc.* **2006**, *128*, 7594–7607.

[40] V. A. Roytman, D. A. Singleton, *J. Am. Chem. Soc.* **2020**, *142*, 12865–12877.

[41] B. R. Ussing, D. A. Singleton, *J. Am. Chem. Soc.* **2005**, *127*, 2888–2899.

[42] B. K. Carpenter, J. N. Harvey, D. R. Glowacki, *Phys. Chem. Chem. Phys.* **2015**, *17*, 8372–8381.

[43] L. M. M. Quijano, D. A. Singleton, *J. Am. Chem. Soc.* **2011**, *133*, 13824–13827.

[44] Y. Oyola, D. A. Singleton, *J. Am. Chem. Soc.* **2009**, *131*, 3130–3131.

[45] J. O. Bailey, D. A. Singleton, *J. Am. Chem. Soc.* **2017**, *139*, 15710–15723.

[46] H. A. Kramers, *Physica* **1940**, *7*, 284–304.

[47] R. F. Grote, J. T. Hynes, *J. Chem. Phys.* **1980**, *73*, 2715.

[48] H. Sumi, T. Asano, *Electrochim. Acta* **1997**, *42*, 2763–2777.

[49] Y. Y. Chuang, D. G. Truhlar, *J. Am. Chem. Soc.* **1999**, *121*, 10157–10167.

[50] D. Aherne, V. Tran, B. J. Schwartz, *J. Phys. Chem. B* **2000**, *104*, 5382–5394.

[51] V. Tran, B. J. Schwartz, *J. Phys. Chem. B* **1999**, *103*, 5570–5580.

[52] R. Garcia-Meseguer, B. K. Carpenter, S. Wiggins, *Chem. Phys. Lett. X* **2019**, *3*, 100030.

[53] R. Garcia-Meseguer, B. K. Carpenter, *European J. Org. Chem.* **2019**, *2019*, 254–266.

[54] F. G. Klärner, B. Krawczyk, V. Ruster, U. K. Deiters, *J. Am. Chem. Soc.* **1994**, *116*, 7646–7657.

[55] Frank-Gerrit Klärner, Frank Wurche, *J. für Prakt. Chemie* **2000**, *342*, 609–636.

[56] B. Chen, R. Hoffmann, R. Cammi, *Angew. Chemie - Int. Ed.* **2017**, *56*, 11126–11142.

[57] M. J. Frisch, G. W. Trucks, H. B. Schlegel, G. E. Scuseria, M. A. Robb, J. R. Cheeseman, G. Scalmani, V. Barone, B. Mennucci, G. A. Petersson, et al., *Gaussian 16, Revision A. 03, Gaussian*, **2016**.

[58] N. L. Allinger, Y. H. Yuh, J. H. Lii, *J. Am. Chem. Soc.* **1989**, *111*, 8551–8566.

[59] J. H. Lii, N. L. Allinger, *J. Am. Chem. Soc.* **1989**, *111*, 8566–8575.

[60] J. H. Lii, N. L. Allinger, *J. Am. Chem. Soc.* **1989**, *111*, 8576–8582.

[61] D. R. Glowacki, A. J. Orr-Ewing, J. N. Harvey, *J. Chem. Phys.* **2015**, *143*, 44120.

[62] J. A. Rackers, Z. Wang, C. Lu, M. L. Laury, L. Lagardère, M. J. Schnieders, J. P. Piquemal, P. Ren, J. W. Ponder, *J. Chem. Theory Comput.* **2018**, *14*, 5273–5289.

[63] G. M. Torrie, J. P. Valleau, *J. Comput. Phys.* **1977**, *23*, 187–199.

[64] S. Kumar, J. M. Rosenberg, D. Bouzida, R. H. Swendsen, P. A. Kollman, *J. Comput. Chem.* **1992**, *13*, 1011–1021.

[65] K. Black, P. Liu, L. Xu, C. Doubleday, K. N. Houk, *Proc. Natl. Acad. Sci. U. S. A.* **2012**, *109*, 12860–12865.

[66] O. Acevedo, W. L. Jorgensen, *J. Chem. Theory Comput.* **2007**, *3*, 1412–1419.

[67] G. Bussi, T. Zykova-Timan, M. Parrinello, *J. Chem. Phys.* **2009**, *130*, 074101.

[68] W. C. Swope, H. C. Andersen, P. H. Berens, K. R. Wilson, *J. Chem. Phys.* **1982**, *76*, 637.

[69] A. Nemkevich, H. B. Bürgi, M. A. Spackman, B. Corry, *Phys. Chem. Chem. Phys.* **2010**, *12*, 14916–14929.

[70] H. C. Andersen, *J. Comput. Phys.* **1983**, *52*, 24–34.

[71] K. Nam, X. Prat-Resina, M. Garcia-Viloca, L. S. Devi-Kesavan, J. Gao, *J. Am. Chem. Soc.* **2004**, *126*, 1369–1376.

[72] E. Neria, M. Karplus, *Chem. Phys. Lett.* **1997**, *267*, 23–30.

[73] N. Kanaan, M. Roca, I. Tuñón, S. Martí, V. Moliner, *J. Phys. Chem. B* **2010**, *114*, 13593–13600.

[74] J. J. Ruiz-Pernía, I. Tuñón, V. Moliner, J. T. Hynes, M. Roca, *J. Am. Chem. Soc.* **2008**, *130*, 7477–7488.

[75] S. Essafi, J. N. Harvey, *J. Phys. Chem. A* **2018**, *122*, 3535–3540.

[76] G. T. Dunning, D. R. Glowacki, T. J. Preston, S. J. Greaves, G. M. Greetham, I. P. Clark, M. Towrie, J. N. Harvey, A. J. Orr-Ewing, *Science* **2015**, *347*, 530–533.

[77] X. Zhang, S. A. Vázquez, J. N. Harvey, *J. Chem. Theory Comput.* **2021**, *17*, 1277–1289.

[78] K. Zinovjev, I. Tuñón, *Wiley Interdiscip. Rev. Comput. Mol. Sci.* **2018**, *8*, e1329.